



Glacial-to-deglacial reservoir and ventilation ages on the southwest Iberian continental margin



Blanca Ausín ^{a, b,*}, Michael Sarnthein ^c, Negar Haghipour ^{b, d}

^a Geology Department, Salamanca University, Pza/Cádidos, s/n, Salamanca, Spain

^b Geological Institute, ETH Zürich, Sonneggstr. 5, 8092, Zurich, Switzerland

^c Institute of Geosciences, University of Kiel, Olshausenstr. 40, 24098, Kiel, Germany

^d Laboratory of Ion Beam Physics, ETHZ, Otto-Stern Weg 5, HPK, 8093, Zurich, Switzerland

ARTICLE INFO

Article history:

Received 10 November 2020

Received in revised form

12 January 2021

Accepted 12 January 2021

Available online 6 February 2021

Handling Editor: A. Voelker

Keywords:

Radiocarbon

Shackleton sites

Last glacial maximum

Heinrich stadial

Deglaciation

Atlantic ocean circulation

ABSTRACT

Detailed assessments of past changes in surface and deep ocean reservoir ages are required to obtain robust ^{14}C -based chronologies of planktic foraminifera and provide insights into ocean circulation changes and the C cycle. Here, we use plateau tuning on foraminiferal ^{14}C data from a sediment core retrieved from the 'Shackleton Sites', a benchmark region for paleoceanographic studies, to i) develop a high-resolution record of surface water reservoir ages, ii) estimate "raw" apparent ventilation ages at two bottom water depths (3150 and 2650 mwd), and iii) establish robust age control for the last 23 ka. Our results provide new insights into the rapid changes in surface and deep-ocean reservoir ages that occurred over the last glacial maximum and last deglaciation. Marine reservoir ages contrast with previous estimates, especially for the cold spell Heinrich Stadial 1, and primarily reflect short-term changes in local hydrography. Variations in ventilation age indicate the influence of ^{14}C -depleted, southern-source deep waters and a marked deepening of the settling depth of the highly ventilated Mediterranean Outflow Water during some millennial-scale intervals, much farther than previously assumed.

© 2021 Elsevier Ltd. All rights reserved.

1. Introduction

Surface and deep-ocean reservoir ages have varied significantly in the past, reflecting ocean circulation changes and variations in the carbon cycle [Cook et al., 2009]. A refined understanding of global ocean dynamics during the last deglaciation requires a comprehensive reconstruction of short-term changes in surface water "marine reservoir age" ('MRA' or 'reservoir effects' sensu Alves et al. [2018]) and in "apparent ventilation ages" [Alves et al., 2018; Cook and Keigwin, 2015] of deep waters mostly originating in different and distant oceanic basins. In this sense, the so-called 'Shackleton Sites' on the SW Iberian Margin (NE Atlantic Ocean) form a unique location where marine records at different depths can be correlated on centennial-to-millennial time scales with ice-core signals from both poles due to variable and alternating incursions of northern- and southern-sourced deep waters [Shackleton et al., 2004; Shackleton et al., 2000]. Moreover, sites

above 1800 m are bathed nowadays by the Mediterranean Outflow Water (MOW), which transports highly saline and warm waters to the North Atlantic [Ambar, 1983; Reid, 1979]. The sites shape a small-scale benchmark region where a joint assessment of the differential physical and chemical properties of the World Ocean's prominent water masses is feasible.

Available data on past changes in MRA over the last deglaciation from this region are relatively coarse and sparse. MRA were considered typically larger than 1000 ^{14}C yr for cold spells such as Heinrich Stadial 1 (HS1) and Younger Dryas (YD) [Skinner et al., 2014], in accordance with reconstructions north of 50° in the NE Atlantic [Peck et al., 2006; Stern and Lisiecki, 2013; Thornalley et al., 2011; Waelbroeck et al., 2001]. Accordingly, enhanced ageing of North Atlantic surface waters would have paralleled phases of weakened Atlantic Meridional Overturning Circulation (AMOC) [Gherardi et al., 2005; McManus et al., 2004] and was thus ascribed to a reduced formation of North Atlantic Deep Water (NADW) and subsequent southward shift of the subpolar front. During these cold spells, deep-water ventilation in the North Atlantic and likewise at the SW Iberian margin might have been generally lower than during the warmer Last Glacial Maximum (LGM) and Bølling/

* Corresponding author. Geology Department, Salamanca University, Pza/Cádidos, s/n, Salamanca, Spain.

E-mail address: ausin@usal.es (B. Ausín).

Allerød (B/A). This shift was then caused by an incursion of radiocarbon-depleted deep waters of southern origin [Balmer and Sarnthein, 2018; Freeman et al., 2016; Skinner and Shackleton, 2004; Skinner et al., 2014] that penetrated as far as 60°N to compensate for a decreased flux of NADW [Curry et al., 1999; Sarnthein et al., 1994].

Robust constraints on past variations in ventilation and reservoir ages at the Shackleton Sites are, however, hindered by limited temporal resolution and uncertainties in available records. More detailed records are required to rigorously test the proposed parallelism between the subtropical NE Atlantic and high latitudes regarding changes in surface and deep ocean reservoir and ventilation age. Such detailed records of past MRA would also help to assess changes in local air-sea CO₂ exchange and hydrographic conditions linked to large-scale changes in ocean circulation and to more local influences (e.g., coastal upwelling and iceberg melt waters). Yet, estimates of MRA remain controversial in subtropical latitudes, where precise chronostratigraphic alignment with independently dated, high-resolution age scales of ice-cores and nearby speleothem records remains equivocal [Waelbroeck et al., 2019].

Such alignment is frequently based on the implicit but debatable assumption that climate signals recorded in marine records are synchronous with those found in ice cores and/or speleothems from different latitudes and distal locations. Moreover, most of these signals show a broad temporal uncertainty range, with stratigraphic tie points being spaced over 5000 years and more over the Last Glacial Maximum (LGM) and early deglacial times. In this regard, radiocarbon plateau-tuning (i.e., tuning of local planktic radiocarbon plateaus to the globally reproducible suite of atmospheric ¹⁴C plateaus) has emerged as a robust tool to: i) constrain past rapid changes in MRA, and ii) to provide accurate age control for marine sediment sections at semi-millennial-scale resolution [Sarnthein et al., 2015; Sarnthein et al., 2007; Sarnthein et al., 2020]. This is achieved by means of suites of atmospheric ¹⁴C plateau boundaries being age-calibrated (cal.) with age uncertainties of <100 yr in a section less than 29 cal ka old of the Lake Suigetsu sediment record [Bronk Ramsey et al., 2020; Bronk Ramsey et al., 2012]. In this study, we establish a ~200-yr-resolution ¹⁴C record for core SHAK06-5K (~51 ¹⁴C dates from 11 to 24 cal. ka) from the Shackleton Sites region, and we employ the plateau-tuning technique to quantitatively determine rapid changes in MRA for the LGM and last deglaciation. Also, we present 14 benthic ¹⁴C dates to assess short-term deglacial changes in apparent ventilation age of deep waters and local circulation changes at 2650 m water depth (mwd). Our results are compared to pertinent data published for deeper neighbor Site MD99-2334 (3150 mwd; Skinner et al., 2014) to provide new insights into the variable advection of northern and southern-source deep waters (i.e., NADW and Antarctic Bottom Water (AABW)), possibly also of MOW.

2. Regional setting

Core SHAK06-5K (37.571 °N, 10.153°W, 2646 mwd) was retrieved from a spur on the upper slope of the SW Iberian margin (Fig. 1) as part of the IODP Site Survey of the Shackleton Sites [Hodell et al., 2014]. Prior Site U1385 was drilled at the same location [Expedition 339 Scientists, 2013], reoccupying the original Shackleton Site MD01-2444 position.

At present, the region is marked by seasonal wind-driven coastal upwelling of subsurface waters during late spring/early summer that mainly consist of the warmer "subtropical" variety of North Atlantic Central Water (NACWst; 100–250 m) and, at strong upwelling events, of NACW of "subpolar" origin (NACWsp; 250–500 m) [van Aken, 2001]. Below, the denser and warmer MOW flows poleward (500–1700 m) overlying the Labrador Sea

Water (LSW), the uppermost component of NADW [Voelker and de Abreu, 2011]. Deeper sites are bathed by Northeastern Atlantic Deep Water (NEADW), consisting of variable contributions of Iceland-Scotland Overflow Water (ISOW), LSW, and Lower Deep Water (LDW). At > 3900 m, LDW, derived from Antarctic Bottom Water (AABW), flows northward, in part due to Coriolis forcing [van Aken, 2001].

3. Material and methods

3.1. Sample preparation and radiocarbon analyses

Between 15 and 30 g of dry sediment was wet sieved through 300- and 250-μm mesh sieves and thoroughly rinsed with MiliQ® water. The 250–300 μm and >300 μm size fractions were immediately dried at 60 °C overnight prior to collection of 35 monospecific samples, containing 45–100 well-preserved specimens of the planktic foraminifera *Globigerina bulloides* from the 250–300 μm fraction (Table 1a), and 13 samples and one duplicate of 1–11 mixed benthic, non-porcelaneous-shell foraminifera from the >250 μm fractions (Table 1b). Samples were measured using an automated system for acid digestion of carbonates [Wacker et al., 2013] and analysis of resulting CO₂ using a gas-accepting ion source installed on a Mini Carbon Dating System (MICADAS) at the Laboratory of Ion Beam Physics, ETH Zurich, enabling ¹⁴C age determination on single foraminifera [Lougheed et al., 2018; Wacker et al., 2013]. Further details on sample preparation and radiocarbon analyses are given in Ausín et al. [2019]. ¹³C/¹²C isotope ratios were used to correct radiocarbon data for isotopic fractionation. To test the accuracy of ¹⁴C measurements standard materials IAEA-C1, IAEA-C2 and coral CSTD were measured in each sequence run. The results were normalized against standard Oxalic Acid II (NIST SRM 4990C) and corrected for radiocarbon blank CO₂ (IAEA C-1) within the range of sample sizes using BATS software V.4.31 [Wacker et al., 2010]. In addition, we considered 18 ¹⁴C ages of *G. bulloides* published by Ausín et al. [2019] for core SHAK06-5K.

3.2. ¹⁴C plateau tuning and choice of a reference record of atmospheric ¹⁴C

The ¹⁴C plateau tuning technique is based on the fast (<10 yr) ¹⁴C exchange between atmosphere and surface ocean, as found by analyses of surface waters after hydrogen bomb tests [Nydal et al., 1980]. Accordingly, the technique requires a continuous reference record of rapid fluctuations in atmospheric ¹⁴C in the past. Back to ~14 cal ka, IntCal20 [Reimer et al., 2020] provides the most recent continuous reference record of atmospheric ¹⁴C in the Northern Hemisphere, being largely based on tree-ring-based ¹⁴C ages. The record shows a suite of periods either marked by ¹⁴C jumps or by 'scatter bands' of nearly-constant ¹⁴C ages, termed ¹⁴C plateaus [Reimer et al., 2020]. From ~14 to 30 cal ka (and beyond), a time span that includes the LGM and early last deglaciation, IntCal20 is based on a combination of ¹⁴C data from speleothems, corals, plant remains in lacustrine sediments and plankton tests in marine sediments, rarely from floating tree-ring records. To integrate this data in a reference framework, IntCal20 incorporates variable, in part unknown, ¹⁴C offsets of marine and speleothem-based ages from the atmosphere. In part, the offsets are derived from ocean circulation models for regions characterized by large-scale MRA variations (e.g., continental margins and upwelling regions) that are not properly resolved in the model [Butzin et al., 2020]. Moreover, IntCal20 is heavily based on the Hulu Cave ¹⁴C record [Cheng et al., 2018; Southon et al., 2012], where short-lived ¹⁴C structures, such as those apparent in the ¹⁴C record of tree-rings back to ~14 cal ka, are filtered out by local effects of unknown

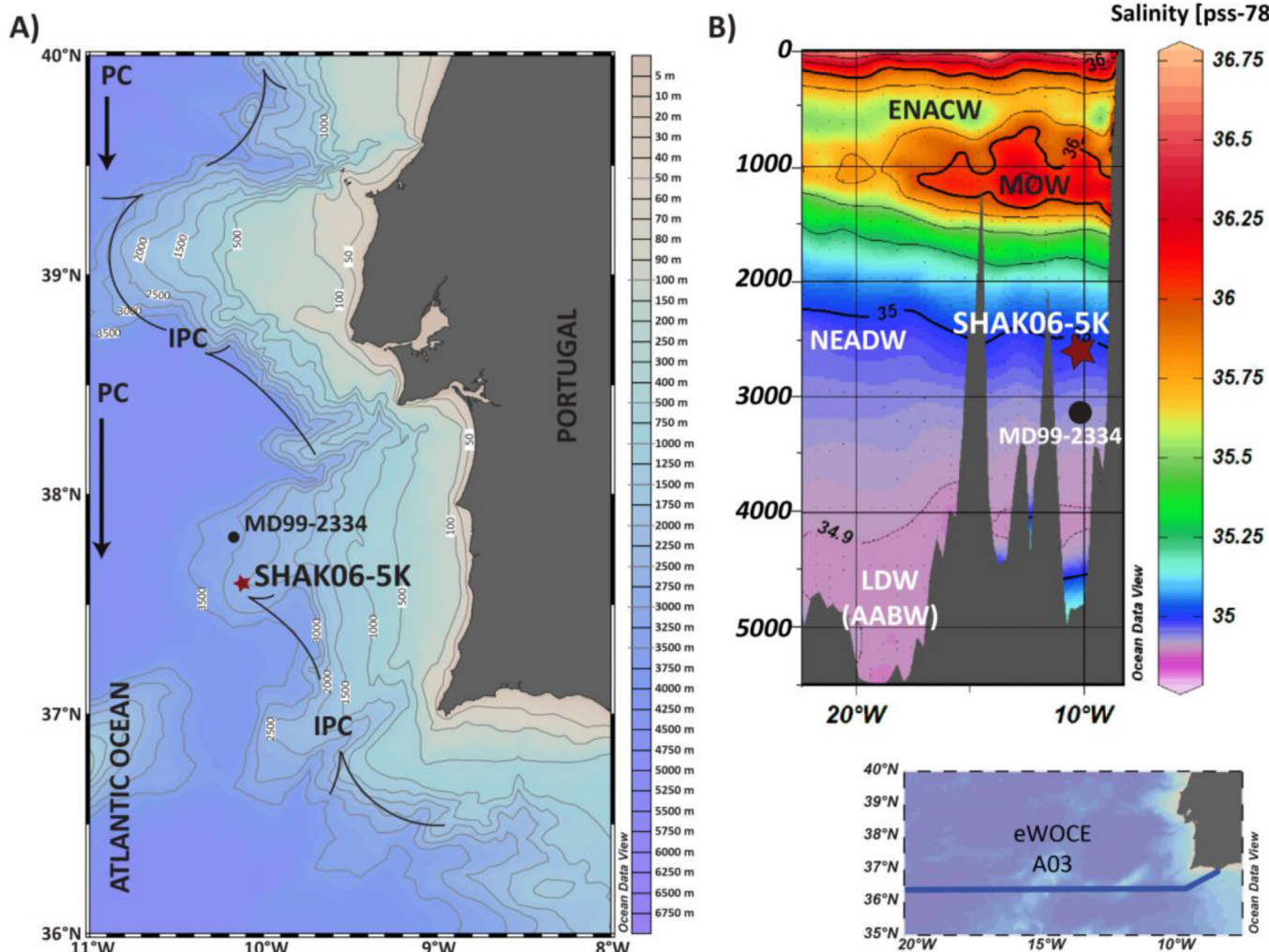


Fig. 1. Study area. A) Surface circulation (black arrows) and location of sediment cores used in this study. PC: Portugal Current. IPC: Iberian Poleward Current. B) Salinity cross section modified from the World Ocean Circulation Experiment (WOCE) transect A03 [Schlitzer, 2000] (<http://www.ewocean.org/>) and depth location of study cores. Water masses were identified following Voelker et al. (2013). ENACW = Eastern North Atlantic Central Water. MOW = Mediterranean Outflow Water. NEADW = Northeastern Atlantic Deep Water. AABW = Antarctic Bottom Water. LDW = Lower Deep Water.

source (e.g., short-term changes in vegetation and soil cover), are not resolved, and/or are largely smoothed [Sarnthein et al., 2020]. As a result, Intcal20 strongly dampens the ^{14}C plateaus for LGM and last deglacial times, negating the ^{14}C plateau tuning approach. In contrast, the atmospheric ^{14}C record from the Japanese Lake Suigetsu sediments is based on fragile plant macrofossils that comprise a high-fidelity archive of atmospheric ^{14}C [Bronk Ramsey et al., 2012]. Their ages show a robust suite of ^{14}C plateaus for LGM and last deglacial times (Fig. S1; Sarnthein et al. [2015;2020]) on the basis of ^{14}C data published by Bronk Ramsey et al. [2012]. Indeed, Suigetsu plateaus closely match the ‘benchmark record’ of tree ring-based ^{14}C plateaus between 10 and ~14 cal ka [Sarnthein et al., 2020]. Farther back until 30 cal ka and beyond, ^{14}C ages of Suigetsu currently provide the only continuous and unsmoothed direct record of atmospheric ^{14}C , where plateau boundaries may be regarded as stratigraphic tie points ‘chiseled in stone’.

Age control of Suigetsu record is based both on microscopy- and XRF-record-based varve counts [e.g., Marshall et al., 2012; Schlosser et al., 2018] and on U/Th-based Bayesian model ages transferred from the Hulu Cave to the Suigetsu record [Bronk Ramsey et al., 2020; Bronk Ramsey et al., 2012]. The U/Th model-based ages are

used as a reference timescale for the assigned ^{14}C plateau boundaries with centennial-to-millennial-scale resolution. The uncertainty associated to the atmospheric cal. age tie points varies between ± 10 and ± 70 cal yr (see Supplementary Text in Sarnthein et al. [2020]). A suite of ^{14}C ages is termed a “ ^{14}C plateau” if these ages form a scatter band with near constant values, where the overall gradient is significantly lower than one ^{14}C year per calendar year, based on visual inspection (Fig. S1 and 2) and/or on objective statistical evaluation by means of the first derivative of all downcore changes in the ^{14}C age – calendar age relationship (Fig. 2; details and software in Sarnthein et al., [2015]). Only ^{14}C plateaus with a duration >250 yr (mostly >300 yr) are considered. The nonparametric 1st-derivative technique uses a running window, mathematically denoted as kernel, which identifies small-scale maxima in the ^{14}C rise over core depth (or calendar age). These ^{14}C jumps help to define plateau boundaries age calibrated in the Suigetsu record. A 1-sigma error band around the slope curve is based on bootstrap resampling [Mudelsee, 2014]. Further details on this technique and the software used have been published elsewhere (Fig. 2 in Sarnthein et al., [2015]). In this study, the record of ^{14}C ages of planktic foraminifera in core SHAK06-5K has a resolution of

Table 1

Conventional radiocarbon age and 1σ error of a) planktic and b) benthic foraminifera samples of core SHAK06-5K. Position of assumed ^{14}C plateau boundaries indicated at core depths as shown in Fig. 2. Data of Ausín et al. [2019] marked by asterisk.

Laboratory code ETH-	Depth (cm)	Species	^{14}C age (yr BP) $\pm 1\sigma$	Plateau name_top/base	Age (cal. ka)
a) Planktic foraminifera samples					
*72991.2.1	82	<i>G. bulloides</i>	11056 \pm 84	Top YD_top	11280
98657.1.1	84	<i>G. bulloides</i>	11106 \pm 85		
96885.1.1	86	<i>G. bulloides</i>	10672 \pm 97	Top YD_base	11760
98656.1.1	88	<i>G. bulloides</i>	11654 \pm 87	YD_top	11870
* 72993.2.1	90	<i>G. bulloides</i>	11437 \pm 86		
98655.1.1	92	<i>G. bulloides</i>	11331 \pm 92		
96884.1.1	94	<i>G. bulloides</i>	11170 \pm 113		
96883.1.1	98	<i>G. bulloides</i>	11575 \pm 95	YD_base	12480
* 70400.1.1	100	<i>G. bulloides</i>	12077 \pm 107		
	103			No name_top	12780
98654.1.1	104	<i>G. bulloides</i>	12223 \pm 89		
98653.1.1	108	<i>G. bulloides</i>	12290 \pm 97	No name_base	13080
* 72995.2.1	110	<i>G. bulloides</i>	12385 \pm 103		
96882.1.1	114	<i>G. bulloides</i>	12901 \pm 145	1a_top	13660
96881.1.1	118	<i>G. bulloides</i>	12952 \pm 95	1a_base	14040
* 72997.2.1	120	<i>G. bulloides</i>	13228 \pm 93	1_top	14160
96880.1.1	124	<i>G. bulloides</i>	13226 \pm 139		
96879.1.1	128	<i>G. bulloides</i>	13298 \pm 90	1_base	15100
*70403.1.1	130	<i>G. bulloides</i>	13615 \pm 109		
96878.1.1	134	<i>G. bulloides</i>	13838 \pm 111	2a_top	15420
98652.1.1	136	<i>G. bulloides</i>	13936 \pm 98		
98651.1.1	138	<i>G. bulloides</i>	13979 \pm 100		
* 72999.2.1	140	<i>G. bulloides</i>	14089 \pm 104		
	141			2a_base/2b_top	16520
96877.1.1	142	<i>G. bulloides</i>	14338 \pm 108		
* 75043.1.1	146	<i>G. bulloides</i>	14290 \pm 101		
96876.1.1	148	<i>G. bulloides</i>	14167 \pm 102	2b_base	16930
* 73001.2.1	152	<i>G. bulloides</i>	14884 \pm 105	3_top	17500
* 73002.2.1	160	<i>G. bulloides</i>	14924 \pm 108		
96875.1.1	164	<i>G. bulloides</i>	15114 \pm 109		
96874.1.1	168	<i>G. bulloides</i>	15075 \pm 142	3_base	18220
* 73003.2.1	172	<i>G. bulloides</i>	15346 \pm 115		
98649.1.1	174	<i>G. bulloides</i>	15524 \pm 111		
98648.1.1	178	<i>G. bulloides</i>	15773 \pm 113		
* 73005.2.1	180	<i>G. bulloides</i>	15978 \pm 138		
96873.1.1	184	<i>G. bulloides</i>	16162 \pm 116	4_top	18650
73007.1.1	190	<i>G. bulloides</i>	16179 \pm 247		
96872.1.1	192	<i>G. bulloides</i>	16360 \pm 126		
* 75044.1.1	196	<i>G. bulloides</i>	16636 \pm 120		
96871.1.1	198	<i>G. bulloides</i>	16413 \pm 128	4_base	19590
* 75016.1.1	200	<i>G. bulloides</i>	17067 \pm 120	5a_top	19720
98647.1.1	204	<i>G. bulloides</i>	17257 \pm 125		
* 75018.1.1	210	<i>G. bulloides</i>	17292 \pm 123		
75045.1.1	214	<i>G. bulloides</i>	17242 \pm 122		
	215			5a_base/5b_top	20240
98646.1.1	216	<i>G. bulloides</i>	17835 \pm 129		
* 75020.1.1	220	<i>G. bulloides</i>	17427 \pm 142		
96870.1.1	222	<i>G. bulloides</i>	17530 \pm 129		
98645.1.1	224	<i>G. bulloides</i>	17870 \pm 128	5b_base	20900
96869.1.1	228	<i>G. bulloides</i>	18128 \pm 160		
* 75022.1.1	230	<i>G. bulloides</i>	18634 \pm 176	6a_top	21000
75046.1.1	234	<i>G. bulloides</i>	18305 \pm 130		
	239			6a_base/6b_top	21890
*75024.1.1	240	<i>G. bulloides</i>	18736 \pm 134		
96868.1.1	244	<i>G. bulloides</i>	187706 \pm 171		
98644.1.1	248	<i>G. bulloides</i>	18849 \pm 136	6b_base	22300
70406.1.1	260	<i>G. bulloides</i>	19979 \pm 181		
b) Benthic foraminifera samples					
108778.1.1	86	<i>Bulimina spp. and Gyroidina spp.</i>	12353 \pm 99		11760
108777.1.1	92	<i>Bulimina spp.</i>	11991 \pm 187		12114
108776.1.1	104	<i>Bulimina spp.</i>	12641 \pm 153		12930
108775.1.1	114	<i>Bulimina spp.</i>	13333 \pm 148		13850
108774.1.1	118	<i>Bulimina spp.</i>	13574 \pm 121		
108772.1.1	120	<i>Bulimina spp.</i>	13849 \pm 109		14160
108773.1.1	120	<i>Cibicidoides spp. and Cibicides wuellerstorfi</i>	13724 \pm 114		
108771.1.1	138	<i>Melonis spp. and Cibicidoides spp.</i>	15165 \pm 281		16049
108770.1.1	142	<i>Melonis spp.</i>	15054 \pm 164		16579
108768.1.1	160	<i>Cibicides wuellerstorfi</i>	15983 \pm 349		18040
108767.1.1	168	<i>Melonis spp. and Uvigerina spp.</i>	16409 \pm 232		
108766.1.1	196	<i>Melonis spp. and Cibicides wuellerstorfi</i>	17748 \pm 191		19456
108765.1.1	220	<i>Melonis spp. and Cibicidoides spp.</i>	18106 \pm 232		21445
108764.1.1	244	<i>Uvigerina spp. and Melonis spp.</i>	19519 \pm 327		22118

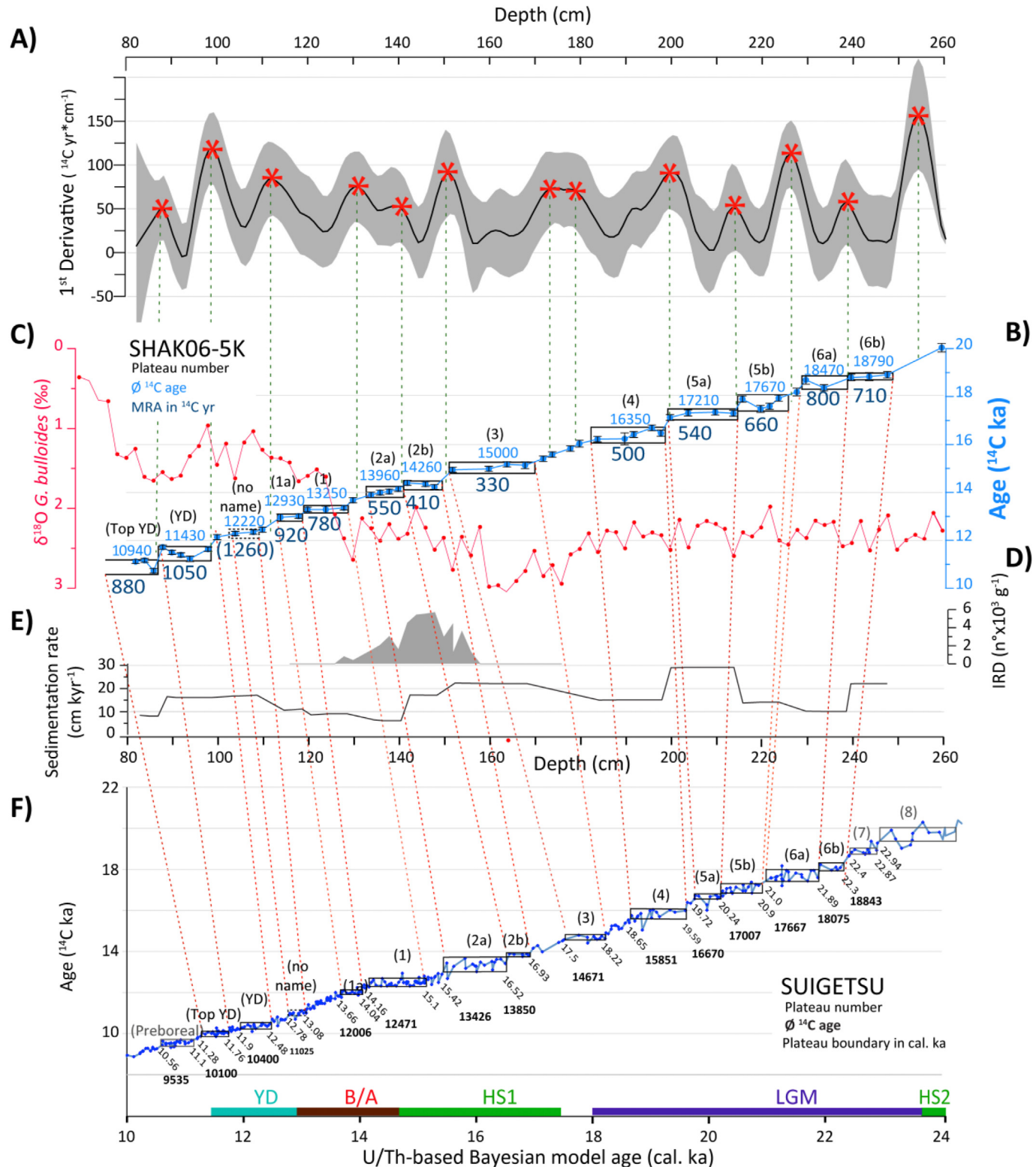


Fig. 2. ¹⁴C plateau tuning of planktic ¹⁴C record from core SHAK06-5K with atmospheric ¹⁴C record from SUIGETSU. A) 1st derivative and 1 σ uncertainty range in grey. 1st derivatives >50 to >100 yr indicate ¹⁴C jumps, marked by a green dash line in B) Planktic ¹⁴C ages (blue dots) and their analytical uncertainty, ¹⁴C plateaus (black rectangles), mean planktic ¹⁴C age of each plateau (black numbers), and marine reservoir ages (blue numbers). C) Planktic oxygen isotope ($\delta^{18}\text{O}$, red solid line; Ausín et al. [2019]) and D) Ice Rafted Debris (IRD, grey shadow; Ausín et al. [2020]) records of SHAK05-5K. ¹⁴C plateau numbers in B are deduced by visual correlation with F) atmospheric ¹⁴C ages from Lake Suigetsu (blue dots), corresponding atmospheric ¹⁴C plateaus (black rectangles; Sarnthein et al. [2020]), and age control points (cal. ka) plotted versus U/Th-based model ages of Bronk Ramsey et al. [2012]. YD = Younger Dryas, B/A = Bølling-Allerød, HS1 and HS2 = Heinrich Stadial 1 and 2, LGM = Last Glacial Maximum. Atmospheric ¹⁴C ages and corresponding uncertainties from Lake Suigetsu are detailed in Figure S1. (For interpretation of the references to colour in this figure legend, the reader is referred to the Web version of this article.)

~200 yr or better. It was tuned by means of statistically estimating the 1st derivative of all downcore changes in the ^{14}C age–calendar age relationship.

3.3. Derivation of reservoir and ventilation age estimates

Surface water reservoir ages were calculated as the difference between pertinent mean atmospheric and planktic ^{14}C plateau ages obtained from Lake Suigetsu core SG062012 and core SHAK06-5K, respectively (Table 2). ‘Raw’ deep ocean ventilation ages at 2646 mwd were calculated by adding the difference between paired benthic and planktic foraminifera ^{14}C ages to the planktic ^{14}C reservoir age [Cook and Keigwin, 2015] (Table 3). Uncertainties in planktic ^{14}C reservoir age (MRA) are calculated by Gaussian error propagation including the 1.68σ uncertainties (considering 90% of all ^{14}C dates) of coeval averaged atmospheric and marine ^{14}C plateaus as well as the average of the measurement error of each planktic ^{14}C date. Similarly, calculation of uncertainties of apparent ventilation ages include the uncertainty of the corresponding MRA and the analytical error of benthic ^{14}C dates. Benthic ventilation ages at 3146 mwd were derived from neighbor Site MD99-2334K, where precise age control and local MRA were deduced by tuning the local ^{14}C planktic ages to those of nearby site SHAK06-5K. MRA were added to benthic-planktic ^{14}C age differences of MD99-2334K published by Skinner et al. [2014].

4. Results

4.1. Foraminifera ^{14}C ages

Radiocarbon ages for 53 planktic and 13 benthic foraminifera samples are listed in Tables 1a and 1b, respectively.

4.2. Structures in the planktic ^{14}C record and results of ^{14}C plateau tuning

The suite of planktic ^{14}C plateaus is regarded continuous and closely reproducing the complete suite of 13 atmospheric radiocarbon plateaus and jumps defined at Suigetsu between 11 and 22.3 cal ka (Top YD – Plateau 6b) (Fig. 2, Table S2 in Sarnthein et al. [2015]). The match also includes the relative length and internal structure of each single plateau, with the exception of the base of Plateau 6a, whose exact identification would require higher data resolution. Core SHAK06-5K shows the twofold positive $\delta^{18}\text{O}$ excursion widely reproduced for the YD, being matched by two subsequent ^{14}C plateaus such as at Suigetsu. Except for 5 cm-long plateaus 1a and Top YD all plateaus comprise sediment sections of >8–20 cm that exceed the general depth of homogenous bioturbational mixing in marine sediments marked by enhanced flux of organic carbon (6–9 cm [Bard, 2001; Trauth et al., 1997];). The suite of ^{14}C plateaus is not paired with any groups of aberrant

Table 2

^{14}C plateau boundaries and marine reservoir ages (MRA) and associated 1.68σ uncertainty at SHAK06-5K. MRA and associated uncertainties are rounded to the next ten. Uncertainties of U/Th-based model ages for atmospheric plateau boundaries are lower than ± 70 yr (see Supplementary Text in Sarnthein et al. [2020]).

Suigetsu plateau no.	Plateau top		Plateau base		$\varnothing^{14}\text{C}$ Age of ^{14}C Plateau (^{14}C yr) $\pm 1.68\sigma$	MRA of ^{14}C plateaus (^{14}C yr)	MRA uncertainty (^{14}C yr)
	U/Th-model-based age (cal. yr)	Depth (cm)	U/Th-model-based age (cal. yr)	Depth (cm)			
Top YD	11280	82	11760	86	10945 ± 400	880	+420/-410
YD	11870	88	12480	98	11433 ± 184	1050	+270/-240
No name	12780	103	13080	108	12197 ± 184	1260	+180/-200
1a	13660	114	14040	118	12926 ± 161	920	+220
1	14160	120	15100	128	13251 ± 69	780	+230
2a	15420	134	16520	141	13961 ± 122	550	+310
2b	16520	141	16930	148	14265 ± 149	410	+210
3	17500	152	18220	168	14999 ± 132	330	+230
4	18650	184	19590	198	16350 ± 185	500	+330
5a	19720	200	20240	215	17215 ± 118	540	+250
5b	20240	215	20900	224	17666 ± 259	660	+390
6a	21000	230	21890	239	18470	800	?
6b	21890	239	22300	248	18785 ± 98	710	+300

Table 3

Raw deep-water ventilation ages at Sites SHAK06-5K and MD99-2334 and uncertainties. Age control and MRA based on ^{14}C plateau stratigraphy of SHAK06-5K (Table 2). B=Benthic. P=Planktic. Data from Skinner et al. [2014] is marked by an asterisk. Ventilation ages and uncertainties are rounded to the next ten. Cal. ages were derived from linear interpolation of sediment depths between age tie points tuned to atmospheric tie points as defined in Fig. 2.

Age (cal. MRA from SHAK06-5K (^{14}C yr))	Core MD99-2334 (3150 mwd)				Core SHAK06-5K (2650 mwd)			
	\varnothing Planktic $^{14}\text{C} \pm 1\sigma$ (^{14}C yr)*	\varnothing Benthic $^{14}\text{C} \pm 1\sigma$ (^{14}C yr)*	B-P (^{14}C yr)	Ventilation age $\pm 1.68\sigma$ (^{14}C yr)	\varnothing Planktic $^{14}\text{C} \pm 1\sigma$ (^{14}C yr)	\varnothing Benthic ^{14}C B-P (^{14}C yr)	Ventilation age $\pm 1.68\sigma$ (^{14}C yr)	
11760 885	10812 ± 50	12180 ± 70	1368	$2250 + 430/-420$	10944 ± 84	12353 ± 99	1408	$2290 + 430/-420$
12114 1053	11181 ± 50	11990 ± 100	809	$1860 + 290/-260$	11433 ± 92	11991 ± 187	558	$1610 + 330/-300$
12930 1256					12196 ± 184	12641 ± 153	444	$1700 + 240/-250$
13850 920	12685 ± 110	13290 ± 130	605	1530 ± 260	12926 ± 116	13454 ± 135	528	1450 ± 260
14160 780	13231 ± 41	14670 ± 80	1439	2220 ± 250	13250 ± 124	13786 ± 112	535	1320 ± 260
16049 555	13919 ± 163	15940 ± 150	2021	2580 ± 340	13960 ± 137	15165 ± 281	1204	1760 ± 410
16579 415	14228 ± 43	15920 ± 90	1692	2110 ± 230	14264 ± 145	15054 ± 164	789	1200 ± 270
18040 328	15146 ± 44	16650 ± 90	1504	1830 ± 250	14999 ± 161	16196 ± 291	1197	1530 ± 370
19456 499	16253 ± 47	17620 ± 100	1367	1870 ± 340	16349 ± 192	17748 ± 191	1398	1900 ± 380
20607 659	17534 ± 49	19030 ± 120	1496	2150 ± 410				
21445 803	18542 ± 53	20260 ± 130	1718	$2520 \pm ?$	17665 ± 221	18106 ± 232	440	1100 ± 450
22118 710	18805 ± 102	20315 ± 155	1510	2220 ± 340	18785 ± 244	19519 ± 327	734	1440 ± 440

outliers, which suggests a lack of Zoophycos burrows that may introduce strong biases in foraminiferal ^{14}C age estimates in specific sediment horizons [Küssner et al., 2018; Leuschner et al., 2002; Löwemark and Grootes, 2004]. As result of ^{14}C plateau tuning, core SHAK06-5K reveals fairly constant high sedimentation rates that average near ~15 cm/kyr (Fig. 2). Minimum (6 cm/kyr) rates are found during the upper HS1 (16.5–15.4 cal ka), whereas maximum sedimentation (27–29 cm/kyr) occurs during late LGM (20.3–19.7 cal. ka) and the top of B/A (13.1–12.8 cal. ka). Prior work on core SHAK06-5K likewise suggests that the impact of bioturbation on the ^{14}C ages of *G. bulloides* was negligible during the last deglaciation [Ausín et al., 2019]. Altogether, these observations suggest that *G. bulloides*-based ^{14}C plateau boundary ages in SHAK06-5K provide a high-resolution and robust record of atmospheric ^{14}C plateaus in ocean surface waters off southwest Portugal.

4.3. Surface water reservoir ages (MRAs)

MRAs vary progressively between 330 and 1200 ^{14}C yr (Table 2 and Fig. 2). Minimum reservoir ages of 330–550 ^{14}C yr apply to plateaus 4–2a spanning the period from 19.6 to 15.4 cal ka, including most of HS1. High surface reservoir ages of 800 ^{14}C yr (plateau 6a) occur about 22–21 cal ka, the mid of LGM, and culminate during plateaus 1a–YD varying from 920 to 1260 yr, that is from mid-B/A to the top of the YD, ~14–11.8 cal. ka.

4.4. Apparent deep-water reservoir ages

Sparse data from core SHAK06-5K suggest (raw) apparent benthic ventilation ages of 1440 and 1100 ^{14}C yr for LGM bottom waters at ~2650 mwd near 22.1 and 21.5 cal ka, respectively,

followed by 1900 ^{14}C yr at 19.5 cal ka (Fig. 3). Subsequently, we find a progressive decrease, culminating with a ventilation age of 1200 ^{14}C yr at 16.6 cal ka (i.e., the middle of HS1). After a short-term high of 1760 ^{14}C yr at 16 cal ka, the deep-water ventilation age shows a second low of 1320 ^{14}C yr at 14.2 cal ka, followed by initially a slow, and then finally an abrupt deep-water aging up to 2290 ^{14}C yr at 11.8 cal. ka.

Core MD99-2334 records raw ventilation ages at 3150 mwd, 500 m deeper than site SHAK06-5K. Ages of >2500 ^{14}C yr mark poor deep-water ventilation during mid-LGM near 21.5 cal. ka. Late LGM ventilation ages decreased gradually down to 1830 yr near 18 cal ka, the onset of HS1. Subsequently, a further maximum of ~2600 ^{14}C yr marks the second half of HS1, near 16 cal ka, paralleling the short-term high recorded at site SHAK06-5K. Minimum ventilation ages of ~1500 ^{14}C yr occur at site MD99-2334 during B/A, followed by an aging by 700 yr over the YD. Over this time, ventilation ages and trends of change are identical at both sites.

5. Discussion

5.1. Surface water reservoir ages (MRAs)

Changing MRAs at site SHAK06-5K indicate significant changes in the origin and dynamics of surface waters over the Iberian margin. Planktic reservoir ages progressively alternate between ~1200 yr and ~350 yr, reflecting gradual shifts in air-sea gas exchange and stratification vs. ocean mixing, along with the influence of regional upwelling and differential ventilation of upwelled waters, which imply a variable thickness of the mixed layer.

Elevated MRAs of 800–660 ^{14}C yr during mid-LGM (22.3–20.2 cal. ka) gradually drop to 500 yr 20.2–18.5 cal ka and

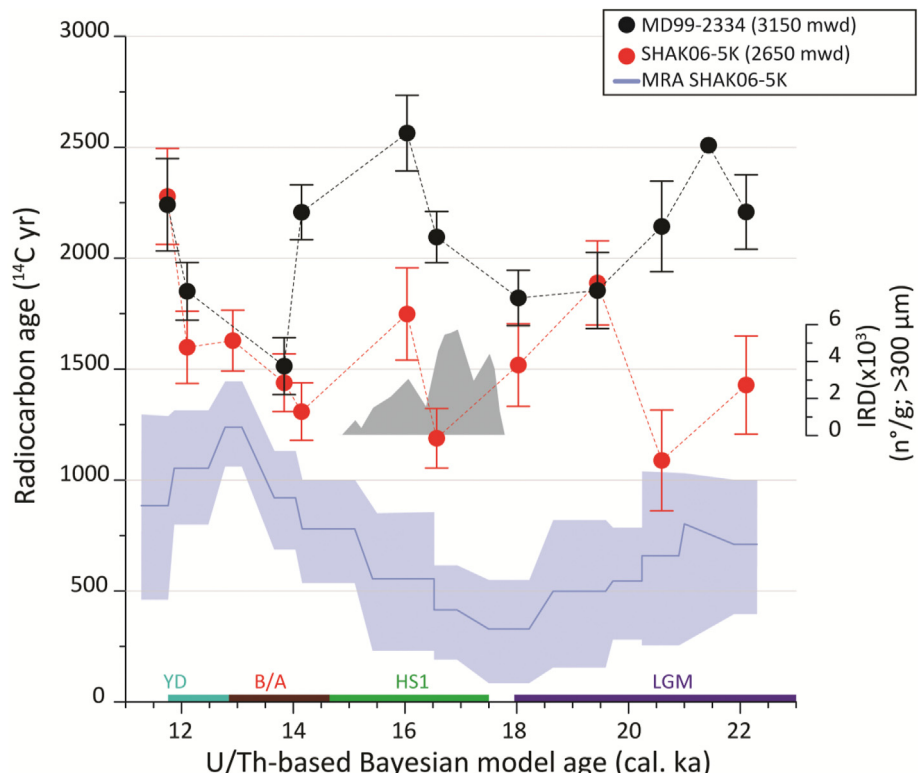


Fig. 3. Changes in raw ‘apparent’ bottom-water ventilation for cores MD99-2334 (black) and SHAK06-5K (red) as compared to MRA at the SW Iberian margin (blue) versus cal. age. Shadowed blue envelope represents 1.68 σ MRA uncertainty. IRD record of SHAK06-5K is shown in grey [Ausín et al., 2020]. (For interpretation of the references to colour in this figure legend, the reader is referred to the Web version of this article.)

are attributed to a slight, gradual decrease in coastal upwelling, as suggested by nanno- and microfossil accumulation rates in the study area [Abrantes, 2000; Palumbo et al., 2013; Salgueiro et al., 2010; Voelker et al., 2009]. Specifically, nannofossil-based proxies from core SHAK06-5K indicate productivity increase and nutricline shoaling ascribed to enhanced upwelling over mid LGM [Ausín et al., 2020]. These MRAs are lower than previous “best-guess” estimates of ~ 1150 ^{14}C yr $\pm >400$ yr [Skinner et al., 2014], and more similar to the MRA of 900 ± 200 ^{14}C yr assumed by Freeman et al. [2016].

During HS1 (17.5–14.7 cal. ka), MRAs of 330–530 ^{14}C yr reflect surface waters that are well ventilated, consistent with the suppression of upwelling during this cold spell [Ausín et al., 2020; Incarbona et al., 2010; Pailler and Bard, 2002; Salgueiro et al., 2010; Voelker et al., 2009]. Enhanced dust transport from the Sahara at that time [Moreno et al., 2002] indicates greater influence of southerly winds favorable for downwelling. Moreover, a paramount coeval maximum of ice-raftered debris (IRD) (Fig. 2b) reflects the arrival of less-saline iceberg melt waters linked to Laurentide ice-sheet instability [Vidal et al., 1997]. Enhanced surface water stability is also reflected by various oceanographic proxy records, e.g., a distinct planktic $\delta^{18}\text{O}$ depletion linked to lower sea surface salinity from 17.8 to 15.2 cal ka (Fig. 2). This feature also applies to other cores nearby in this region that at this time were closer to the Portuguese shoreline due to lower sea level [Ausín et al., 2020; Bard et al., 2000; Cayre et al., 1999; Eynaud et al., 2009; Voelker and de Abreu, 2011]. Thus, both surface wind trajectories and melt water-induced surface water stability may have effectively precluded upwelling of ^{14}C -depleted subsurface waters from below.

The low reservoir ages of SHAK06-5K estimated for HS1 contrast with the high reservoir age (1900 ^{14}C yr) at 17.6 cal ka and a subsequent decrease postulated for nearby core MD99-2334 [Skinner et al., 2014]. The proximity of the two core sites, the duration of HS1, and the magnitude of the difference in MRA estimates preclude local hydrography as a cause for this discrepancy. Instead, limitations may exist in age control of the MD99-2334 record imposed by (i) the chronostratigraphic alignments of the $\delta^{18}\text{O}$ record of MD99-2334 to the Hulu Cave speleothem and to the North Greenland Ice Core Project (NGRIP) ice-core chronology. Based on different viable alignments, Skinner et al. [2014] provided “best-guess” and “maximum and minimum likely” reservoir ages between 20 and 14 cal ka, resulting in a large envelope of possibilities. (ii) The Hulu Cave atmospheric ^{14}C record is based on the implicit assumption that the Dead Carbon Fraction (DCF) has remained constant [Southon et al., 2012], while past changes in monsoonal rainfall patterns on millennial time scales may result in variations in DCF [Kong et al., 2005]. The “minimum likely” MRA of 745–490 ^{14}C yr proposed by Skinner et al. [2014] appears most consistent with our estimates. Moreover, these “minimum likely” estimates were found to be more consistent with MRA reconstructions for the LGM period [Freeman et al., 2016].

Our chronology, based on ^{14}C plateau tuning, assigns the onset of fast deglacial planktic $\delta^{18}\text{O}$ depletion (toward $< 3\%$) observed in both at MD99-2334 and SHAK06-5K cores to 18 cal ka, whereas the “best-guess” chronology of Skinner et al. [2014] dates this onset at ~ 16 cal ka in core MD99-2334. A closer stratigraphic agreement (17.6 cal. ka) was subsequently achieved by aligning the $\delta^{18}\text{O}$ record of core MD99-2334 to the NGRIP dust record [Skinner et al., 2019].

Without undervaluing the significance of previous approaches, the ^{14}C plateau tuning technique poses advantages for high-resolution, robust estimates of MRA, especially in cases where record alignment is not unequivocal.

During HS1, the IRD peak in core SHAK06-5K provides a further line of support for this portion of our chronology and thus, for reduced reservoir ages (Fig. 2). This peak is a recurrent feature of

marine sequences all over the North Atlantic [Bard et al., 2000; Sierra et al., 2020; Skinner and Shackleton, 2004] and likely reflects Heinrich Event 1.1 (H1.1) identified in the North Atlantic, previously dated between 15.5 and 17.1 cal ka [Hodell et al., 2017]. In our record, the prime IRD maximum of core SHAK06-5K is centered at ~ 16.5 – 16.8 cal ka, well within the 2-sigma uncertainty range reported by Hodell et al. [2017]. In contrast, the “best-guess chronology” for core MD99-2334, which implied a MRA of 1200 ^{14}C yr, placed the local twin IRD peak, at 15.5 cal. ka.

Our low estimate for reservoir ages over HS1 is in line with ages of 600 ($+400/-300$) ^{14}C yr deduced after reevaluating data from a stack of numerous cores in the North Atlantic including the Iberian margin [Stern and Lisiecki, 2013] for the time span 16.5–16 cal ka, when AMOC strength reached a minimum [Gherardi et al., 2005] and IRD a maximum. The authors ascribed these low MRA to enhanced upper-water column stratification primarily due to iceberg melting-waters and the subsequent enhanced air-sea equilibration, a scenario also supported by model results [Ritz et al., 2008].

Over B/A, the rise of MRA is ascribed to enhanced upwelling of ^{14}C -depleted subsurface waters, as corroborated by multiple paleoproductivity records in this region [Ausín et al., 2020; Incarbona et al., 2010; Pailler and Bard, 2002; Palumbo et al., 2013]. Widening of upwelling cells as far as the study-site location was attributed to the intensification of northeasterly winds at that time, linked to the strengthening of the Azores anticyclonic cell [Incarbona et al., 2010; Pailler and Bard, 2002]. Additionally, the subsequent northward expansion of the subtropical gyre and northward displacement of the Azores Front [Schwab et al., 2012] may have favored a front-induced upwelling at the study site [Ausín et al., 2020; Palumbo et al., 2013].

Starting at the onset of the YD (Fig. 3), reservoir ages off SW Portugal gradually decrease in accordance with a progressive reduction of upwelling and deepening of the nutricline, as recorded by multiple proxies in core SHAK06-5K [Ausín et al., 2020].

5.2. Bottom water ventilation ages

“Apparent” ventilation ages (in ^{14}C yr) roughly indicate the time elapsed since deep waters were in contact with the surface ocean and the atmosphere, and observed changes are generally interpreted in the context of changes in ocean thermohaline circulation. The term “apparent” reflects three major unknowns: the actual site and distance of past deep-water formation, the MRA of downwelled surface waters, and the ventilation age of deep waters laterally admixed from elsewhere. In addition to the benthic ventilation ages obtained for site SHAK06-5K (Fig. 3), the planktic ^{14}C record of nearby site MD99-2334 was tuned to that of site SHAK06-5K and the benthic-planktic age anomalies in core MD99-2334 [Skinner et al., 2014] converted into apparent ventilation ages by adding the local planktic MRA of SHAK06-5K. In this way, we sought to develop a paired record of glacial-to-deglacial ventilation ages for two different depth levels (~ 2650 and ~ 3150 mwd) on the SW Iberian margin (Fig. 3).

During terminal LGM (19.5–18.5 cal. ka), the Iberian continental margin below ~ 2650 m depth was bathed by poorly ventilated deep waters (~ 2000 ^{14}C yr old), a value that contrasts with modern values of 800–900 ^{14}C yr (equivalent to a ‘circulation age’ of >300 ^{14}C yr; Matsumoto, 2007). While the geometry of overturning of NADW during the LGM was probably similar to that of today [Keigwin and Swift, 2017; Sarnthein et al., 2020], the LGM rise of ventilation ages by ~ 1200 ^{14}C yr at MD99–2334 may suggest a general weakening and slight shoaling of NADW [Freeman et al., 2016], and subsequently enhanced influence of ^{14}C -depleted southern-source water masses (i.e., AABW). Due to Coriolis forcing,

however, these waters were closely confined to the East Atlantic continental margin, as indicated by coeval ventilation ages, as low as 350–670 yr, obtained from similar water depths at Mid-Atlantic Ridge site MD08-3180 [Balmer and Sarnthein, 2018]. Intermediate ventilation ages (1900–1100 ^{14}C yr) of upper bottom waters at ~2650 mwd off the SW Portuguese margin suggest that occasional admixtures of AABW with NADW during early and mid-LGM reached far upslope, farther than previously assumed [Freeman et al., 2016].

During HS1, ventilation ages near 3150 m reached a further maximum of 2580 ^{14}C yr, similar to that near 21.5 cal. ka. Accordingly, ‘old’ southern-source waters continued to dominate the Iberian continental margin near 3150 mwd over HS1 [Skinner and Shackleton, 2006], when deep-water formation in the North Atlantic was generally weakened [McManus et al., 2004]. Unlike the LGM, however, the extent and age of this maximum in ventilation age matched an analogous maximum in ventilation age at Site MD08-3180 (3064 m) west of the Azores Islands [Balmer and Sarnthein, 2018]. This large-scale coherence in ventilation ages suggests a complete filling of the northeast Atlantic basin by southern-source waters. Because of Coriolis forcing, some remnants of NADW may then have possibly streamed into the West Atlantic basin only [Thornalley et al., 2011].

In sharp contrast to the ventilation age increase to ~2100 and up to 2600 ± 340 ^{14}C yr, that southern-source deep waters show at MD99-2334 during HS1 (17.5–14.7 cal ka), bottom waters at SHAK06-5K show an enigmatic drop in ventilation age to ages down to 1200 ± 270 ^{14}C yr near 16.6 cal ka, an age well constrained by the age tie point of the top of ^{14}C Plateau 2a (Figs. 2 and 3). To explain the immense local deep-water rejuvenation at 2650 m, we suggest that inherently young Mediterranean Outflow Waters (MOW), today confined to 500–1800 m at the Iberian continental margin, may then have played a fundamental role through short-term deep injection and turbulent mixing with waters farther below. During Heinrich stadials the relative buoyancy of MOW was further reduced under the influence of major aridification of the Mediterranean realm [Bartov et al., 2003; Sánchez-Goñi et al., 2002]. Moreover, it was driven by a large density reduction of major North Atlantic water masses, primarily due to surface water freshening in the Nordic Seas at times of reduced AMOC and/or even a phase of AMOC “shutdown” [Rogerson et al., 2012]. During this time, MOW may have cascaded to depths at least to 1600–2200 m, as suggested by dual lines of sediment proxy evidence, namely (epi-) benthic foraminifera assemblages, and epi-benthic $\delta^{13}\text{C}$ values [Schönfeld and Zahn, 2000; Zahn et al., 1987]. The influence of nepheloid layers linked to deeper parts of MOW during HS1 was also suggested to account for the advection and deposition of fine and coarse silt sediments to the study site [Magill et al., 2018]. Sierro et al. [2020] has recently provided detailed documentation that a deepening of the MOW plume was a short-lived event during HS1, synchronous to the IRD peak in layer H1.1. Likewise, our results show minimum ventilation ages coeval with the IRD peak H1.1 near 16.6 cal ka (Fig. 3). Following this scenario, a local denser-than-modern plume of MOW could descend to >2600 m, down to the top of AABW.

At the end of HS1 (near 15.1 cal. ka), concomitant to a shoaling of MOW [sensu Sierro et al., 2020], ventilation age records of both sites SHAK06-5K and MD99-2334 vary in concert, showing almost identical values. Ventilation ages of deep waters that were 300–800 yr lower at 2650 mwd than at 3150 mwd indicate a sudden minor admixture of old AABW up to 2650 mwd in parallel with the trend shown by highly ^{14}C depleted lower deeper waters at 3150 mwd.

At 14.2 cal ka, bottom waters show a renewed major

rejuvenation and both sites start to show identical ventilation ages (~1500 ^{14}C yr) at 13.8 ka cal, concomitant to a return to strong North Atlantic overturning and NADW formation over the B/A [Gherardi et al., 2005; McManus et al., 2004]. This provides further indirect evidence for the major reorganization of deep-water flows during HS1 times of reduced and/or inverted North Atlantic overturning. Finally, the end of the YD (~11.8 cal. ka) was marked at both sites by a general increase in ventilation age up to 2100 ^{14}C yr, possibly explained by a further northward expansion of southern-source deep waters up to the study site, possibly linked to the coeval sudden weakening of AMOC [Gherardi et al., 2005].

6. Conclusions

- A 100–200-yr resolution planktic foraminiferal ^{14}C record from the SW Iberian margin enabled us to define a suite of ~20 age tie points with semi-millennial resolution that were tuned to age-calibrated boundaries of Suigetsu atmospheric ^{14}C plateaus between 11 and 24 cal. ka.
- Marine reservoir ages (MRA) of surface waters have been deduced from the ^{14}C age difference of coeval planktic and atmospheric ^{14}C plateaus. Local MRA vary between 300 and 1200 ^{14}C yr over the LGM and last deglaciation, and reflect past changes in hydrography over the northeastern Atlantic continental margin. Our record of surface water reservoir ages contrasts with previous MRA estimates from the SW Iberian margin, especially for the LGM and the HS1 and YD cold intervals, and implies larger influence of regional changes in oceanography.
- Ventilation ages of deep waters suggest minor influence of AABW near 2650 mwd as compared to deeper waters (~3150 mwd) for the Early and mid-LGM, and similar ventilation patterns for the late LGM and late deglaciation
- During the HS1 cold interval, however, coeval with a major ice rafted debris peak, high ventilation ages suggest a major incursion of southern-source deep waters at 3150 mwd in contrast to bottom water ages of 1200–1300 yr farther above. These ages may reflect a major short-term deepening of the penetration of highly ventilated MOW down to >2600 m.

Author statement

Blanca Ausín: contributed equally to discussion and writing.
Michael Sarnthein: contributed equally to discussion and writing.
Negar Haghipour: assisted with radiocarbon analyses.

Data statement

All original data used in this study, necessary to understand, evaluate, and replicate this research are available in the public repository PANGAEA® under <https://doi.pangaea.de/10.1594/PANGAEA.921812>.

Declaration of competing interest

The authors declare that they have no known competing financial interests or personal relationships that could have appeared to influence the work reported in this paper.

Acknowledgements

We would like to thank Editor Antje Voelker, and Patrick Rafter and an anonymous reviewer for their valuable suggestions to improve this manuscript. The authors are deeply grateful to Timothy I. Eglinton for his valuable comments on this contribution

and his continuous and unlimited support. We are indebted to Lukas Wacker for his many years of dedication to improve the methodologies that made radiocarbon analyses of this core possible. We thank Pieter M. Grootes for stimulating discussions, David Hodell for kindly providing access to core material, and Bryan Lougheed for generously sharing unpublished ^{14}C data of core SHAK06-5K, in this way motivating further radiocarbon analyses for this study. Daniel Montluçon and Clayton Magill are acknowledged for their assistance collecting and processing core SHAK06-5K onboard the RSS James Cook. This study was supported by a Postdoctoral Fellowship within the TRAMPOLINE project funded by the Swiss National Science Foundation [200021_175823] and the Ministry of Science, Innovation and Universities (Spain) [RTI 2018-099489-B-100].

Appendix A. Supplementary data

Supplementary data to this article can be found online at <https://doi.org/10.1016/j.quascirev.2021.106818>.

References

- Abrantes, F., 2000. 200 000 yr diatom records from Atlantic upwelling sites reveal maximum productivity during LGM and a shift in phytoplankton community structure at 185 000 yr. *Earth Planet Sci. Lett.* 176, 7–16.
- Alves, E.Q., et al., 2018. The worldwide marine radiocarbon reservoir effect: definitions, mechanisms, and prospects. *Rev. Geophys.* 56, 278–305.
- Ambar, I., 1983. A shallow core of Mediterranean water off western Portugal. *Deep Sea Research Part A. Oceanographic Research Papers* 30, 677–680.
- Ausín, B., et al., 2019. Radiocarbon age offsets between two surface dwelling planktonic foraminifera species during abrupt climate events in the SW Iberian margin. *Paleoceanography and Paleoclimatology* 34, 63–78.
- Ausín, B., et al., 2020. The impact of abrupt deglacial climate variability on productivity and upwelling on the southwestern Iberian margin. *Quat. Sci. Rev.* 230, 106139.
- Balmer, S., Sarnthein, M., 2018. Glacial-to-deglacial changes in North Atlantic meltwater advection and deep-water formation – centennial-to-millennial-scale ^{14}C records from the Azores plateau. *Geochem. Cosmochim. Acta* 236, 399–415.
- Bard, E., 2001. Paleoceanographic implications of the difference in deep-sea sediment mixing between large and fine particles. *Paleoceanography* 16, 235–239.
- Bard, E., et al., 2000. Hydrological impact of Heinrich events in the subtropical northeast Atlantic. *Science* 289, 1321–1324.
- Bartov, Y., et al., 2003. Catastrophic arid episodes in the eastern Mediterranean linked with the north atlantic. Heinrich events. *Geology* 31, 439–442.
- Bronk Ramsey, C., et al., 2020. Reanalysis of the atmospheric radiocarbon calibration record from Lake Suigetsu, Japan. *Radiocarbon* 62, 989–999.
- Bronk Ramsey, C., et al., 2012. A complete terrestrial radiocarbon record for 11.2 to 52.8 kyr B.P. *Science* 338, 370–374.
- Butzin, M., et al., 2020. A short note on marine reservoir age simulations used in IntCal20. *Radiocarbon* 62, 865–871.
- Cayre, O., et al., 1999. Paleoceanographic reconstructions from planktonic foraminifera off the Iberian Margin: temperature, salinity, and Heinrich events. *Paleoceanography* 14, 384–396.
- Cheng, H., et al., 2018. Atmospheric $^{14}\text{C}/^{12}\text{C}$ changes during the last glacial period from Hulu Cave. *Science* 362, 1293–1297.
- Cook, G.T., et al., 2009. Chapter 4 radiocarbon as a tracer in the global carbon cycle. In: Froehlich, K. (Ed.), *Radioactivity in the Environment*. Elsevier, pp. 89–137.
- Cook, M.S., Keigwin, L.D., 2015. Radiocarbon profiles of the NW Pacific from the LGM and deglaciation: evaluating ventilation metrics and the effect of uncertain surface reservoir ages. *Paleoceanography* 30, 174–195.
- Curry, W.B., et al., 1999. Millennial-scale changes in ventilation of the thermocline, intermediate, and deep waters of the glacial North Atlantic. In: Clark, P.U., et al. (Eds.), *Mechanisms of Global Climate Change at Millennial Time Scales*, pp. 59–76.
- Eynaud, F., et al., 2009. Position of the Polar Front along the western Iberian margin during key cold episodes of the last 45 ka. *G-cubed* 10 (n/a-n/a).
- Freeman, E., et al., 2016. An Atlantic–Pacific ventilation seesaw across the last deglaciation. *Earth Planet Sci. Lett.* 424, 237–244.
- Gherardi, J.M., et al., 2005. Evidence from the Northeastern Atlantic basin for variability in the rate of the meridional overturning circulation through the last deglaciation. *Earth Planet Sci. Lett.* 240, 710–723.
- Hodell, D.A., et al., 2014. The JC089 Scientific Party, JC089 Cruise Report - IODP Site Survey of the Shackleton Sites, SW Iberian Margin. British ocean data Centre, Rep. https://www.bodc.ac.uk/data/information_and_inventories/cruise_inventory/report/13392/.
- Hodell, D.A., et al., 2017. Anatomy of Heinrich Layer 1 and its role in the last deglaciation. *Paleoceanography* 32, 284–303.
- Incarbón, A., et al., 2010. Primary productivity variability on the Atlantic Iberian Margin over the last 70,000 years: evidence from coccolithophores and fossil organic compounds. *Paleoceanography* 25, PA2218, 2210.1029/2008PA001709.
- Keigwin, L.D., Swift, S.A., 2017. Carbon isotope evidence for a northern source of deep water in the glacial western North Atlantic. *Proc. Natl. Acad. Sci. Unit. States Am.* 114, 2831–2835.
- Kong, X., et al., 2005. Complicated responses of stalagmite $\delta^{13}\text{C}$ to climate change during the last glaciation from Hulu Cave, Nanjing, China. *Sci. China Earth Sci.* 48, 2174–2181.
- Küssner, K., et al., 2018. High-resolution radiocarbon records trace episodes of Zoophycos burrowing. *Mar. Geol.* 403, 48–56.
- Leuschner, D.C., et al., 2002. Possible influence of Zoophycos bioturbation on radiocarbon dating and environmental interpretation. *Mar. Micropaleontol.* 46, 111–126.
- Lougheed, B.C., et al., 2018. Moving beyond the age–depth model paradigm in deep-sea palaeoclimate archives: dual radiocarbon and stable isotope analysis on single foraminifera. *Clim. Past* 14, 515–526.
- Löwemark, L., Grootes, P.M., 2004. Large age differences between planktic foraminifers caused by abundance variations and Zoophycos bioturbation. *Paleoceanography* 19.
- Magill, C.R., et al., 2018. Transient hydrodynamic effects influence organic carbon signatures in marine sediments. *Nat. Commun.* 9, 4690.
- Marshall, M., et al., 2012. A novel approach to varve counting using μXRF and X-radiography in combination with thin-section microscopy, applied to the Late Glacial chronology from Lake Suigetsu, Japan. *Quat. Geochronol.* 13, 70–80.
- McManus, J.F., et al., 2004. Collapse and rapid resumption of Atlantic meridional circulation linked to deglacial climate changes. *Nature* 428, 834.
- Moreno, A., et al., 2002. Saharan dust transport and high-latitude glacial climatic variability: the Alboran Sea record. *Quat. Res.* 58, 318–328.
- Mudelsee, M., 2014. *Climate Time Series Analysis: Classical Statistical and Bootstrap Methods*. Springer.
- Nydal, R., et al., 1980. Transfer of bomb ^{14}C to the ocean surface. *Radiocarbon* 22, 626–635.
- Pailler, D., Bard, E., 2002. High frequency palaeoceanographic changes during the past 140 000 yr recorded by the organic matter in sediments of the Iberian Margin. *Palaeogeogr. Palaeoclimatol. Palaeoecol.* 181, 431–452.
- Palumbi, E., et al., 2013. Abrupt variability of the last 24 ka BP recorded by coccolithophore assemblages off the Iberian Margin (core MD03-2699). *J. Quat. Sci.* 28, 320–328.
- Peck, V.L., et al., 2006. High resolution evidence for linkages between NW European ice sheet instability and Atlantic Meridional Overturning Circulation. *Earth Planet Sci. Lett.* 243, 476–488.
- Reid, J.L., 1979. On the contribution of the mediterranean sea outflow to the Norwegian-Greenland sea, *deep sea research Part A. Oceanographic Research Papers* 26, 1199–1223.
- Reimer, P.J., et al., 2020. The IntCal20 northern Hemisphere radiocarbon age calibration curve (0–55 cal kBP). *Radiocarbon* 62, 725–757.
- Ritz, S.P., et al., 2008. Modeling the effect of abrupt ocean circulation change on marine reservoir age. *Earth Planet Sci. Lett.* 268, 202–211.
- Rogerson, M., et al., 2012. Paleoceanography of the Atlantic-Mediterranean exchange: overview and first quantitative assessment of climatic forcing. *Rev. Geophys.* 50.
- Salgueiro, E., et al., 2010. Temperature and productivity changes off the western Iberian margin during the last 150 ky. *Quat. Sci. Rev.* 29, 680–695.
- Sánchez-Góñi, M., et al., 2002. Synchronicity between marine and terrestrial responses to millennial scale climatic variability during the last glacial period in the Mediterranean region. *Clim. Dynam.* 19, 95–105.
- Sarnthein, M., et al., 2015. Planktic and benthic ^{14}C reservoir ages for three ocean basins, calibrated by a suite of ^{14}C plateaus in the glacial-to-deglacial Suigetsu atmospheric ^{14}C record. *Radiocarbon* 57, 129–151.
- Sarnthein, M., et al., 2007. ^{14}C reservoir ages show deglacial changes in ocean currents and carbon cycle. In: Schmittner, A., et al. (Eds.), *Ocean Circulation: Mechanisms and Impacts - Past and Future Changes of Meridional Overturning*. American Geophysical Union, Washington, DC, pp. 175–196.
- Sarnthein, M., et al., 2020. Plateaus and jumps in the atmospheric radiocarbon record – potential origin and value as global age markers for glacial-to-deglacial paleoceanography, a synthesis. *Clim. Past Discuss* 16, 1–25.
- Sarnthein, M., et al., 1994. Changes in east Atlantic deepwater circulation over the last 30,000 years: eight time slice reconstructions. *Paleoceanography* 9, 209–267.
- Scholz, G., et al., 2018. An extended and revised Lake Suigetsu varve chronology from ~50 to ~10 ka BP based on detailed sediment micro-facies analyses. *Quat. Sci. Rev.* 200, 351–366.
- Schönfeld, J., Zahn, R., 2000. Late Glacial to Holocene history of the Mediterranean Outflow. Evidence from benthic foraminiferal assemblages and stable isotopes at the Portuguese margin. *Palaeogeogr. Palaeoclimatol. Palaeoecol.* 159, 85–111.
- Schwab, C., et al., 2012. Coccolithophore paleoproductivity and ecology response to deglacial and Holocene changes in the Azores Current System. *Paleoceanography* 27.
- Shackleton, N.J., et al., 2004. Absolute calibration of the Greenland time scale: implications for Antarctic time scales and for $\Delta^{14}\text{C}$. *Quat. Sci. Rev.* 23, 1513–1522.
- Shackleton, N.J., et al., 2000. Phase relationships between millennial-scale events 64,000–24,000 years ago. *Paleoceanography* 15, 565–569.
- Sierro, F.J., et al., 2020. Mediterranean Overflow over the last 250 kyr: freshwater

- forcing from the tropics to the ice sheets. *Paleoceanography and Paleoclimatology* 35, e2020PA003931.
- Skinner, L.C., et al., 2019. Marine reservoir age variability over the last deglaciation: implications for marine CarbonCycling and prospects for regional radiocarbon calibrations. *Paleoceanography and Paleoclimatology* 34, 1807–1815.
- Skinner, L.C., Shackleton, N.J., 2004. Rapid transient changes in northeast Atlantic deep water ventilation age across Termination I. *Paleoceanography* 19.
- Skinner, L.C., Shackleton, N.J., 2006. Deconstructing Terminations I and II: revisiting the glacioeustatic paradigm based on deep-water temperature estimates. *Quat. Sci. Rev.* 25, 3312–3321.
- Skinner, L.C., et al., 2014. Radiocarbon evidence for alternating northern and southern sources of ventilation of the deep Atlantic carbon pool during the last deglaciation. *Proc. Natl. Acad. Sci. Unit. States Am.* 111, 5480–5484.
- Southon, J., et al., 2012. A high-resolution record of atmospheric ^{14}C based on Hulu Cave speleothem H82. *Quat. Sci. Rev.* 33, 32–41.
- Thornalley, D.J.R., et al., 2011. The deglacial evolution of north atlantic deep convection. *Science* 331, 202–205.
- Trauth, M.H., et al., 1997. Bioturbational mixing depth and carbon flux at the sea-floor. *Paleoceanography* 12, 517–526.
- van Aken, H.M., 2001. The hydrography of the mid-latitude Northeast Atlantic Ocean — Part III: the subducted thermocline water mass. *Deep Sea Res. Oceanogr. Res. Pap.* 48, 237–267.
- Vidal, L., et al., 1997. Evidence for changes in the north atlantic deep water linked to meltwater surges during the Heinrich events. *Earth Planet Sci. Lett.* 146, 13–27.
- Voelker, A.H.L., de Abreu, L., 2011. A review of abrupt climate change events in the northeastern Atlantic Ocean (iberian margin): latitudinal, longitudinal, and vertical gradients. In: *Abrupt Climate Change: Mechanisms, Patterns, and Impacts*, pp. 15–37.
- Voelker, A.H.L., et al., 2009. Hydrographic conditions along the western Iberian margin during marine isotope stage 2. *G-cubed 10 (n/a-n/a)*.
- Wacker, L., et al., 2010. MICADAS: routine and high-precision radiocarbon dating. *Radiocarbon* 52, 252–262.
- Wacker, L., et al., 2013. Towards radiocarbon dating of single foraminifera with a gas ion source. *Nucl. Instrum. Methods Phys. Res. Sect. B Beam Interact. Mater. Atoms* 294, 307–310.
- Waelbroeck, C., et al., 2001. The timing of the last deglaciation in North Atlantic climate records. *Nature* 412, 724–727.
- Waelbroeck, C., et al., 2019. Consistently dated Atlantic sediment cores over the last 40 thousand years. *Scientific Data* 6, 165.
- Zahn, R., et al., 1987. Benthic isotope evidence for changes of the Mediterranean outflow during the Late Quaternary. *Paleoceanography* 2, 543–559.